Electrochemical behaviour of thorium(IV) in molten LiF–CaF_2 medium on inert and reactive electrodes

P. Chamelot, L. Massot*, L. Cassayre, P. Taxil

Université de Toulouse, INPT, UPS, Laboratoire de Génie Chimique, Département Procédés Electrochimiques, F-31062 Toulouse Cedex 09, France, CNRS, Laboratoire de Génie Chimique, F-31062 Toulouse Cedex 09, France

A B S T R A C T

The electrochemical behaviour of the Th(IV)/Th system was examined in molten LiF–CaF_2 medium on inert (molybdenum), reactive (nickel) and liquid (bismuth) electrodes in the 810–920 °C temperature range by several electrochemical techniques. Experimental results showed that (i) thorium fluoride was reduced in a single step exchanging 4 electrons and limited by thorium ions diffusion in the solution, (ii) the oxide ions induce the precipitation of Th(IV) in the form of thorium oxide (ThO_2), in a process involving as intermediate compound a soluble oxifluoride ($ThOF_2$), (iii) the reduction of thorium ions on reactive (Ni and liquid Bi) electrodes yields compounds Ni–Th and Bi–Th with a potential shift of around 0.7 V (for Ni and Bi) more anodic than the reduction of Th(IV) on inert substrate.

1. Introduction

In the frame of the Generation IV International Forum (GIF) [1], the selection of the most promising nuclear reactors has been done. One of the systems is the molten salt fast reactor (MSFR) concept, characterized by a fast neutron spectrum, which could be operated in simplified and safe conditions in the Th/^{233}U fuel cycle with fluoride salts [2]. The initial fuel salt is composed of LiF–ThF_4–(heavy nuclide)F_3 with 77.5 mole% of LiF, this fraction being kept constant during reactor operation. The main originality of this concept is the use of molten salts both as the fuel and the coolant, including the on-line reprocessing of the salt to be performed with the aim to remove the fission products that poison the neutronic reaction in the core.

The MSFR concept is strengthen by the technologies developed in molten fluoride media between 1954 and 1976 at Oak Ridge National Laboratory (ORNL) [3]. The technical feasibility of the concept has been demonstrated with the construction and operation of the molten salt reactor experiment between 1964 and 1969 [4–6]. However, the reprocessing unit was not included in this experiment and today remains to be optimised. ORNL worked until 1976 on the molten salt breeder reactor (MSBR) and a complete reprocessing scheme was proposed, including a first step of actinides (Ans) extraction, and a second step of lanthanides (Lns) extraction from the Th-containing salt, by means of metallic transfer of Lns in a chloride salt through a liquid bismuth phase (metallic transfer process) [7]. Much more recently, an evaluation of this process was performed and it was shown [8] that the efficiency of the Th/Ln separation process as proposed by ORNL was very selective, avoiding losses of Th in the reprocessing unit, but very restricted (less than 10% of Lns were extracted).

The low efficiency of the metallic transfer process was acceptable in the frame of the MSBR project, thanks to the high reprocessing speed of the salt (typically, all the salt was planned to be reprocessed in 10 days in order to ensure a maximal breeding ratio of the concept). At the present time, as the MSFR's neutron spectrum is fast, the capture rate of fission becomes negligible and the reprocessing rate can be significantly decreased [9]. Such changes in the reprocessing strategy imply new requirements, including in particular to strongly increase the Th/Lns separation efficiency. Hence, other techniques than metallic transfer process are conceivable, such as:

The oxide precipitation by additions of a strong oxide donor or by $He + H_2O$ bubbling.
The electroreduction on inert or reactive cathodes.

The assessment of such techniques requires an in-depth knowledge of both chemistry and electrochemistry of Th in fluoride media. The first stage in the view of determining relevant information on the behaviour of Th(IV) in molten salts consists in studying it as a dissolved solute. This allows notably to establish the reduc-

* Corresponding author. Tel.: +33 5 61 55 81 94, fax: +33 5 61 55 61 39.
E-mail address: massot@chimie.ups-tlse.fr (L. Massot).

tion mechanism and the diffusion coefficient of Th(IV), which is not possible when ThF_4 is a major constituent of the solvent. Up to date, most of the electrochemical works carried out on Th in molten salt solutions concerned the measurement of the equilibrium potentials, from which some thermodynamic parameters have been calculated. The majority of the studies have been performed in chloride medium, and two different mechanisms have been proposed with either two [10,11] or one [12–15] reduction steps, the latter involving the existence of a Th(II) electroactive compound:

$$Th(IV) + 2e^- \leftrightarrows Th(II) \quad (1)$$

$$Th(II) + 2e^- \leftrightarrows Th \quad (2)$$

or

$$Th(IV) + 4e^- \leftrightarrows Th \quad (3)$$

In a recent reassessment of the basic electrochemical properties of actinides, Cassayre et al. have indicated that the reduction mechanism of $ThCl_4$ into Th in the molten LiCl–KCl eutectic occurs according to a one step process [16].

In fluoride melts, the mechanism of Th(IV) reduction is not clearly established. Very few studies are published and the proposed mechanism of Th reduction, established on nickel electrodes, corresponds to a single step exchanging 4 electrons [17–19].

The present paper is focused on the electrochemical behaviour of ThF_4 on different substrates (Mo, Ta, Ni and Bi) and on the influence of oxide ion additions in a LiF–CaF_2 solvent. It yields some experimental results to be considered in the view of the MSFR salt reprocessing.

2. Experimental

The cell was a vitreous carbon crucible placed in a cylindrical vessel made of refractory steel and closed by a stainless steel lid cooled by circulating water. The inside part of the walls was protected against fluoride vapours by a graphite liner. The experiments were performed under an inert argon atmosphere (less than 1 ppm O_2), previously dehydrated and deoxygenated using a purification cartridge (air liquide). The cell was heated using a programmable furnace and the temperatures were measured using a chromel–alumel thermocouple. A more detailed description of the set-up can be found in Refs. [20,21].

The electrolytic bath consisted of a eutectic LiF–CaF_2 (Merck 99.99%) mixture (79.5/20.5 molar ratio), initially dehydrated by heating under vacuum (10^{-5} bar) to its melting point (762 °C) for 72 h. Thorium ions were introduced into the bath in the form of ThF_4 (Cerac 99.99%) pellets and oxide ions in the form of Li_2O or CaO (Cerac 99.9%).

Molybdenum, nickel wires (Goodfellow 99.99% 1 mm diameter) and bismuth, for liquid electrode, (Goodfellow 99.99%) were used as working electrodes. The auxiliary electrode was a vitreous carbon (V25) rod (3 mm diameter) with a large surface area (2.5 cm^2).

The potentials were referred to a platinum wire (0.5 mm diameter) immersed in the molten electrolyte, acting as a quasi-reference electrode $Pt/PtO_x/O^{2-}$ [22].

All the electrochemical studies and the electrolysis were performed with an Autolab PGSTAT30 potentiostat/galvanostat controlled with the GPES 4.9 software.

Cyclic voltammetry (CV), chronopotentiometry (CP) and square wave voltammetry (SWV) were the electrochemical techniques used for the investigation of the thorium reduction process.

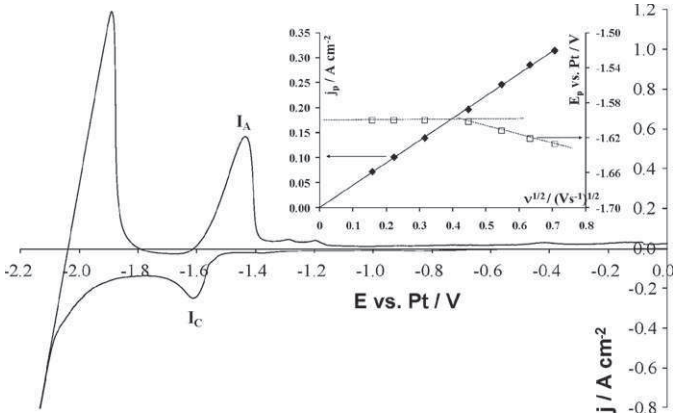

Fig. 1. Cyclic voltammogram of the LiF–CaF_2–Th(IV) (0.041 mol kg^{-1}) system at 100 mV s^{-1} and 840 °C. Working el.: Mo (S = 0.16 cm^2); auxiliary el.: vitreous carbon; comparison el.: Pt. Inset: linear relationship of Th(IV) peak current density (left axis) and reduction peak potential (right axis) vs. the square root of the scanning potential rate at 840 °C. Working el.: Mo (S = 0.16 cm^2); auxiliary el.: vitreous carbon; comparison el.: Pt.

3. Results and discussion

The presentation of the experimental results is divided in two parts:

(i) electrochemical reduction of Th(IV) on an inert electrode first without oxide and then after oxide addition,
(ii) electrochemical reduction on reactive cathodes.

3.1. Th(IV) reduction mechanism on inert electrode

3.1.1. LiF–CaF_2–ThF_4 melts

Cyclic voltammetry was first carried out on inert electrodes (Mo) in the LiF–CaF_2–Th(IV) (0.041 mol kg^{-1}) melt at 840 °C. The cathodic and anodic limits of the electrochemical window correspond to the reduction of Li(I) from the solvent, and the oxidation of the working electrode material (Mo). The cyclic voltammogram, presented in Fig. 1, exhibits one peak I_c in the cathodic run prior to the reduction of the solvent at around −1.62 V vs. Pt. The sharp anodic peak I_a at −1.43 V vs. Pt, observed on the reverse scan, and associated with the cathodic one, is typical of the dissolution of a solid phase deposited during the cathodic run (stripping peak).

Thus, the cathodic reaction is attributed to the following reaction:

$$Th(IV) + 4e^- \leftrightarrows Th$$

At a given temperature, the current density of the reduction peak increases linearly with the thorium fluoride content, as showed in Fig. 2. This linear relationship can be used to determine the concentration of Th(IV) in the melt.

The reversibility of the system has been examined by plotting the influence of the scan rate on the peak potential as presented in the inset of Fig. 1 (right y-axis). This plotting shows that, for scan rate lower than 200 mV s^{-1}, the peak potential is constant, therefore the system can be considered as quasi-reversible.

Then, the linearity of current peak (j_p) vs. square root of the scan rate ($v^{1/2}$) has been verified, on the inset of Fig. 1 (left y-axis), indicating that the electrochemical reduction process was controlled by the diffusion of Th(IV) ions in the solution. Consequently, the theoretical equation, valid for a reversible soluble/insoluble system, can

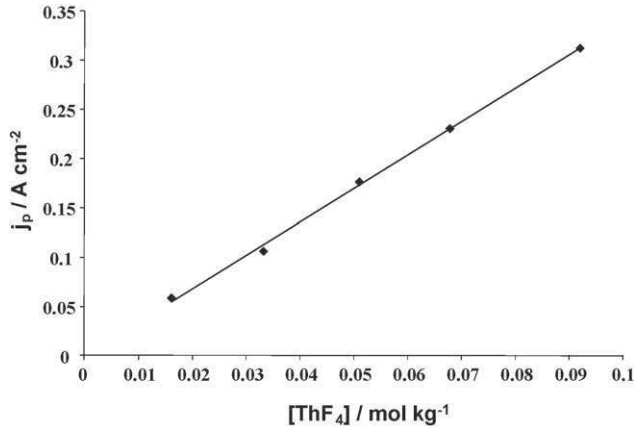

Fig. 2. Linear relationship of the Th(IV) reduction peak current density vs. the Th(IV) concentration in the melt. Scanning potential rate: 100 mV s^{-1} and 840 °C. Working el.: Mo (S = 0.16 cm^2); auxiliary el.: vitreous carbon; comparison el.: Pt.

be used [23]:

$$J_p = -0.61n\ FSC^0\left(\frac{nF}{RT}\right)^{1/2} D^{1/2}\nu^{1/2} \quad (4)$$

where S is the electrode area (cm^2), C^0 is the solute concentration (mol cm^{-3}), D is the diffusion coefficient (cm^2 s^{-1}), F is the Faraday constant, n is the number of exchanged electrons, T is the temperature (K) and ν is the potential scanning rate (V s^{-1}).

The value obtained with the experimental data plotted in Fig. 1 is: $J_p = (0.4469 \pm 0.0003)\nu^{1/2}$.

In the case of metal deposition, cyclic voltammetry is not well adapted to determine the number of exchanged electrons because the nucleation phenomenon causes a deformation of the reduction peak. Alternatively, square wave voltammetry can be used to solve this problem.

Square wave voltammetry: the use of this technique for analytical purposes, theoretically valid for reversible systems, can be extended to other systems as far as the criterion of linearity between the peak intensity and the square root of the frequency signal is respected [24–28]. In the present study, this linearity was observed in the 9–64 Hz frequency range. Fig. 3 shows

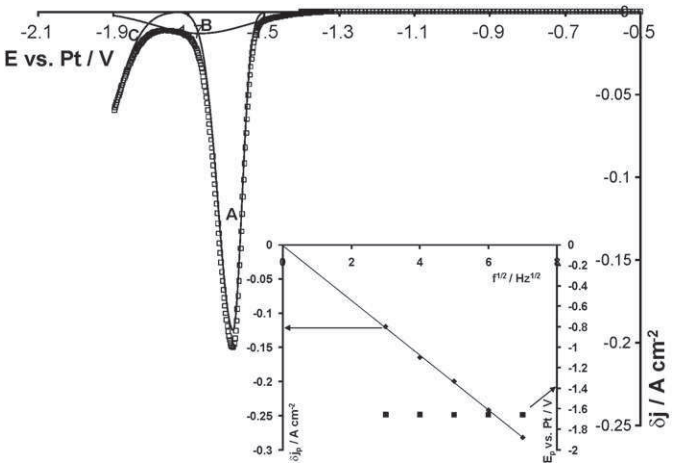

Fig. 3. Square wave voltammogram of the LiF–CaF_2–Th(IV) (0.041 mol kg^{-1}) melt. Frequency: 25 Hz at 840 °C. Working el.: Mo (S = 0.30 cm^2); auxiliary el.: vitreous carbon; comparison el.: Pt. Inset: linear relationship of Th(IV) peak current density (left axis) and reduction peak potential (right axis) vs. the square root of the frequency at 840 °C. Working el.: Mo (S = 0.30 cm^2); auxiliary el.: vitreous carbon; comparison el.: Pt.

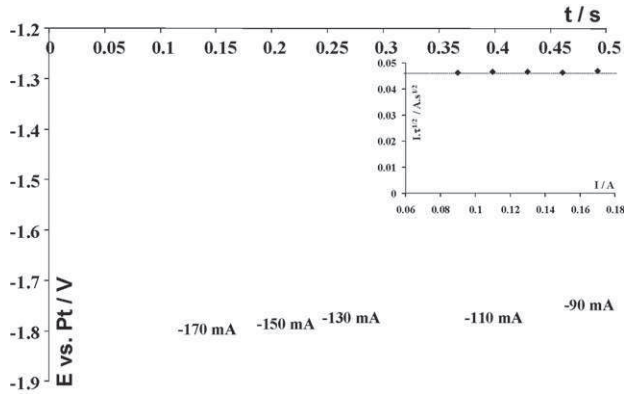

Fig. 4. Typical chronopotentiograms with the intensity of LiF–CaF_2–Th(IV) (0.041 mol kg^{-1}) at 840 °C with ohmic drop correction (R = 0.5 Ω). Working el.: Mo (S = 0.16 cm^2); auxiliary el.: vitreous carbon; comparison el.: Pt. Inset: variation of $I\tau^{1/2}$ vs. the intensity at 840 °C. Working el.: Ta (S = 0.16 cm^2); auxiliary el.: vitreous carbon; comparison el.: Pt.

a typical square wave voltammogram of the LiF–CaF_2–Th(IV) (0.041 mol kg^{-1}) system, at 25 Hz and 840 °C, which exhibits a peak with a quasi-Gaussian shape (peak A), prior to the solvent wave (C). As mentioned in previous papers, the distortion of peak A, regarding to the classical perfectly Gaussian one which is valid for a soluble/soluble system, is due to the currentless nucleation phase of the metal deposition [29,30]. Concerning quasi-reversible systems, Ref. [30] indicates how the measurement of the half-peak width ($W_{1/2}$) allows the number of exchanged electrons to be determined in the case of an asymmetric peak, according to:

$$W_{1/2} = 3.52 \times \frac{RT}{nF} \quad (5)$$

In order to verify the validity of this relation, the reversibility of the system has also been investigated by plotting the peak current density and the peak potential vs. the square root of the signal frequency (see inset of Fig. 3). The linearity of δI_p vs. $f^{1/2}$ and the invariance of E_p with $f^{1/2}$ prove that the system can be considered as quasi-reversible, as stated above with cyclic voltammetry.

From Fig. 3, n was found to have an average value of 3.9 ± 0.1.

Consequently, peak (A) is attributed to the Th(IV) reduction.

Besides, the deconvolution of the SWV suggests the presence of peak B, with very low current density, between the Th(IV) reduction peak (A) and the solvent reduction wave (C). Referring to the system of TaF_7^{2-} reduction in the presence of oxides, previously investigated by our group and detailed in Ref. [27], the peak B may be attributed to the reduction of a thorium oxifluoride compound (presumably $ThOF_2$) due to a residual oxide impurities content in the melt.

This hypothesis is comforted by the recent observation by nuclear magnetic resonance (NMR) measurements of a stable $ThOF_2$ compound in fluoride media [31].

Chronopotentiometry: Fig. 4 presents typical chronopotentiograms of LiF–CaF_2–Th(IV) (0.041 mol kg^{-1}) reduction obtained for several current densities on Mo cathode at 840 °C after correction of ohmic drop (R = 0.5 Ω). Each plot exhibits a single plateau associated with the reduction of Th(IV) into Th in the same potential range as observed in cyclic or square wave voltammetries.

According to the data plotted in the inset of Fig. 4, Sand's equation [32] was verified:

$$J\tau^{1/2} = 0.5nFSC^0\pi D^{1/2} = (0.072 \pm 0.002)As^{1/2} \quad (6)$$

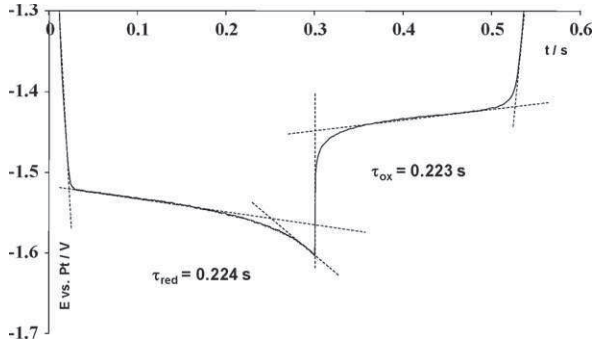

Fig. 5. Reversal chronopotentiogram of ThF_4 (0.101 mol kg^{-1}) in LiF–CaF_2 eutectic, $i = -0.11$ A. Working el.: Mo ($S = 0.30$ cm^2); auxiliary el.: vitreous carbon; comparison el.: Pt.

The reversal chronopotentiogram, presented in Fig. 5, evidences the formation of a solid phase on the electrode during the cathodic run since the transition time of the oxidation and the reduction steps are equals ($\tau_{ox} = \tau_{red}$) [33].

Chronopotentiometric measurements confirm also that the electrochemical reduction process is limited by the diffusion of Th(IV) ions in the melt, allowing the Th(IV) diffusion coefficient to be calculated.

3.1.2. Diffusion coefficient determination

Using Eqs. (4) or (6) with $n = 4$, the Th(IV) diffusion coefficient (D) was calculated. The D value is, whatever the applied methodology, $(5.0 \pm 0.1)\ 10^{-5}$ cm^2 s^{-1} at 840 °C. In the 810–920 °C temperature range, the variation of Ln D vs. the inverse absolute temperature is plotted in Fig. 6. The linear relationship observed between Ln D and $1/T$ proves that the variation of the diffusion coefficient obeys an Arrehnius law, as:

$$D = D^{\circ} exp\left(-\frac{E_a}{RT}\right) \quad (7)$$

where E_a is the activation energy in J mol^{-1}, T is the temperature in K, D is the diffusion coefficient in cm^2 s^{-1}.

The obtained results give the following equation:

$$\mathrm{Ln}\, D = -3.92(\pm 0.03) - \frac{6668.50(\pm 0.03)}{T} \quad (8)$$

From Eqs. (7) and (8), the activation energy is 55.5 ± 0.2 kJ mol^{-1}.

3.1.3. Influence of oxide additions: LiF–CaF_2–ThF_4–CaO melts

The cyclic voltammogram of Fig. 7 of the LiF–CaF_2–Th(IV) (6.84×10^{-2} mol kg^{-1}) system, plotted on Mo electrode at

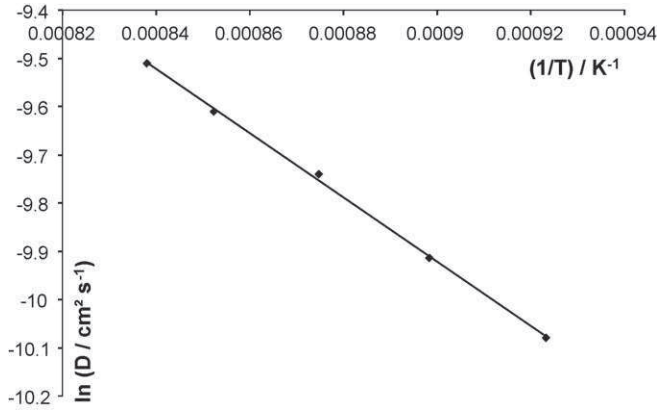

Fig. 6. Variation of the logarithm of the diffusion coefficient vs. the inverse of the absolute temperature.

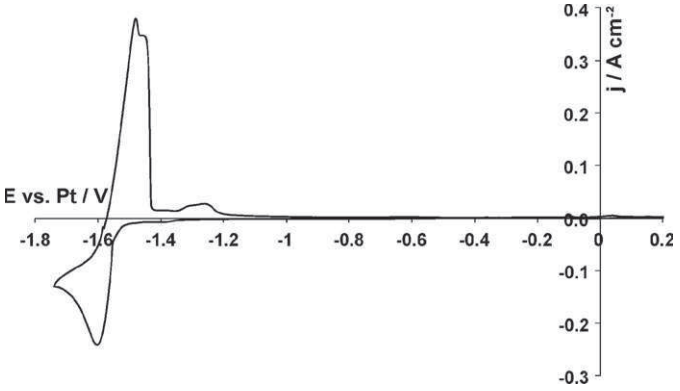

Fig. 7. Cyclic voltammogram of the LiF–CaF_2–Th(IV) (6.84×10^{-2} mol kg^{-1}) system after the addition of CaO (6.00×10^{-2} mol kg^{-1}) at 100 mV s^{-1} and 840 °C. Working el.: Mo ($S = 0.30$ cm^2); auxiliary el.: vitreous carbon; comparison el.: Pt.

100 mV s^{-1} after the addition of oxides CaO (6.00×10^{-2} mol kg^{-1}), always exhibits a single cathodic peak. However, two reoxidation peaks are observed during the reverse scan, suggesting that two reduction products were formed at close potentials during the cathodic scan.

The square wave voltammogram presented in Fig. 8 for the LiF–CaF_2–Th(IV) (6.84×10^{-2} mol kg^{-1})–CaO (6.00×10^{-2} mol kg^{-1}) system confirms this assumption. The experimental plotting $\delta j = f(E)$ exhibits a large enhancement of the current between the Th(IV) reduction peak (A) and the solvent wave (C), compared to Fig. 3. The comparison of the deconvolution of this signal with the one of Fig. 3 highlights the decrease of peak A (4 exchanged electrons) and the increase of peak B (2 exchanged electrons) current densities with oxide addition. These results confirm that peak B is linked to the reduction of the thorium(IV) oxifluoride complex $ThOF_2$, with 2 exchanged electrons, leading to a Th(II) oxide compound, presumably ThO.

Several oxide additions were carried out and, using SWV calibration measurements, the peak A current density allowed the Th(IV) content remaining in the liquid salt phase to be calculated. Fig. 9 shows the variation of the remaining Th(IV) content (left axis) and the peak B current density (right axis) with the oxide content added in the melt. A linear decrease of the remaining Th(IV) content due to the precipitation of Th(IV) is evidenced. The global stoichiometry was determined using the slope of the straight line obtained in Fig. 9 (left axis). The measured slope value was close to −0.49, indicating

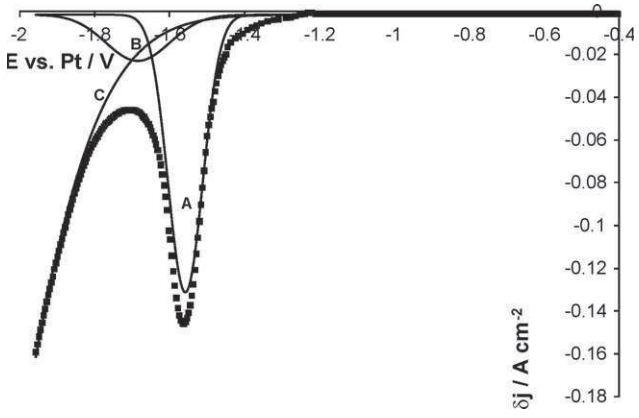

Fig. 8. Square wave voltammogram of the LiF–CaF_2–Th(IV) (6.84×10^{-2} mol kg^{-1}) melt after the addition of CaO (7.90×10^{-2} mol kg^{-1}) frequency: 25 Hz at 840 °C. Working el.: Mo ($S = 0.31$ cm^2); auxiliary el.: vitreous carbon; comparison el.: Pt.

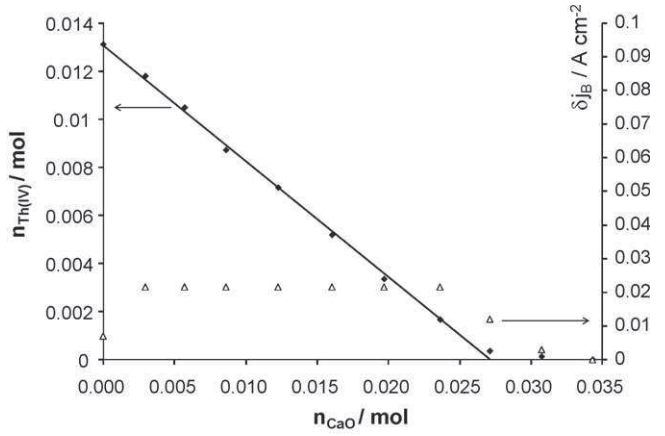

Fig. 9. Variation of the Th(IV) amount in the melt (left axis) and thorium oxifluoride reduction peak current density (right axis) vs. the CaO content added in the melt.

the formation of ThO_2 according to the following reaction:

$$ThF_4 + 2O^{2-} \leftrightarrows ThO_2 + 4F^- \quad (9)$$

It can also be observed that peak B current density increases only during the first oxide addition, then remains constant while Th(IV) is present in the melt, and finally decreases to zero when no more Th(IV) remains in the melt.

So, $ThOF_2$ is intermediate specie in the overall chemical pathway of precipitation of ThF_4 into ThO_2, explaining that, as far as all ThF_4 is not completely precipitated, the amount of $ThOF_2$ remains constant.

The two steps of the precipitation are likely to be:

$$ThF_4 + O^{2-} \leftrightarrows ThOF_2 + 2F^- \quad (10)$$

$$ThOF_2 + O^{2-} \leftrightarrows ThO_2 + 2F^- \quad (11)$$

Afterwards, an excess of oxide precipitates all the thorium in the form of ThO_2.

After cooling, a white layer, presenting a significant radioactivity, was found at the bottom of the solidified salt, as shown in Fig. 10. This layer corresponds to ThO_2 precipitate.

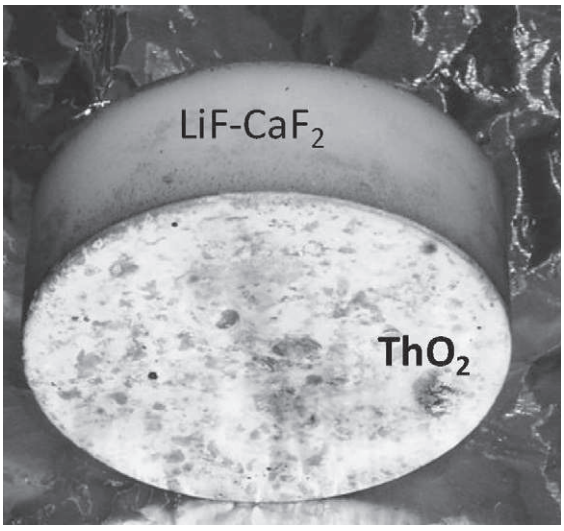

Fig. 10. Photography of the bath pellet, observed after cooling: in light grey $LiF–CaF_2$ and in white ThO_2.

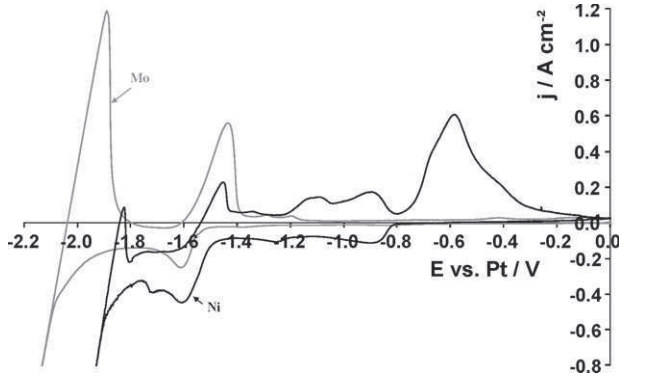

Fig. 11. Comparison of the cyclic voltammograms of $LiF–CaF_2–Th(IV)$ (6.77×10^{-2} mol kg^{-1}) on Mo and Ni electrodes at 100 mV s^{-1} and 840 °C. Auxiliary el.: vitreous carbon; comparison el.: Pt.

3.2. Th(IV) reduction on reactive electrodes

3.2.1. Th(IV) reduction on nickel electrode

It has been demonstrated that the extraction of elements such as lanthanides from Li based fluoride melts is facilitated by the use of a reactive cathode material such as nickel owing to the depolarisation effect caused by nickel alloy formation [34–37]. The depolarisation has been shown to be due to a lowered activity of the electrodeposited element. This technique could be suited to the extraction of Th(IV) since the Ni–Th phase diagram [38] displays 6 solid intermetallic compounds at the operating temperature (840 °C).

Accordingly, the Th(IV) electrochemical behaviour on nickel electrode was examined using cyclic voltammetry. Fig. 11 compares the cyclic voltammograms obtained at 840 °C on nickel and molybdenum electrodes at 100 mV s^{-1}. On nickel electrode, addi-

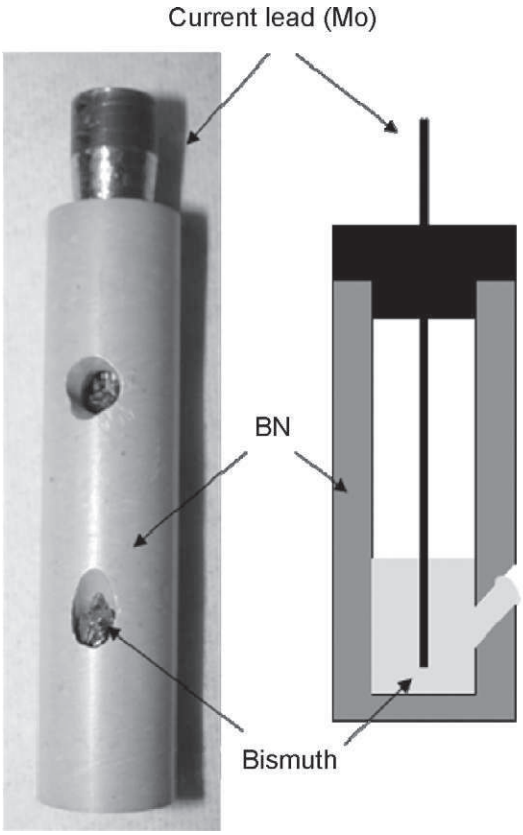

Fig. 12. Scheme and photography of the set-up used for liquid bismuth electrode.

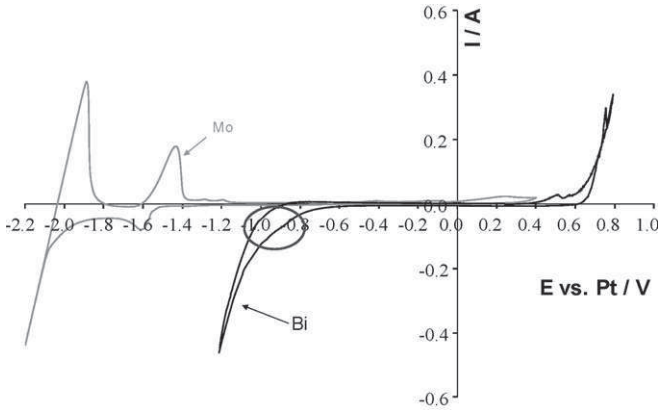

Fig. 13. Comparison of the cyclic voltammograms of LiF–CaF_2–Th(IV) (6.77×10^{-2} mol kg^{-1}) on Mo and liquid Bi electrodes at 100 mV s^{-1} and 840 °C. Auxiliary el.: vitreous carbon; comparison el.: Pt.

tional waves are detected prior to the reduction of Th(IV) into Th metal observed on Ta substrate. Referring to the observations of Clayton et al. on the electrochemical system of Th(IV) in molten fluorides [17], these waves are attributed to the formation of Th–Ni alloys. The potential difference between the solvent reduction and the first wave observed on nickel substrate, corresponding to the alloy formation (around 1.1 V) is greatly increased compared with the one on an inert electrode (around 0.5 V). Thus, it can be assumed that the complete extraction of thorium ions from a Li based fluoride melt will be facilitated by the use of nickel cathode [39].

3.2.2. Th(IV) reduction on liquid bismuth electrode

Another way of decreasing the activity of the electrodeposited metal is the use of a liquid cathode such as Cd, Bi, and Al. Literature deals with results on extraction or separation processes of actinides or lanthanides using mainly Cd and Bi [40,41].

In this work, the behaviour of liquid Bi, which has a low melting point (271 °C) and a high density (10.05) at melting temperature, was investigated.

A specific technical change of the experimental set-up, detailed in Fig. 12, was needed in order to operate with a liquid pool as working electrode: the bismuth was placed in a boron nitride (MCSE, quality AX05 oxide free) compartment with an open window in the BN wall immersed in the melt. The electrical contact was obtained using a molybdenum wire, insulated with boron nitride, immersed in the liquid.

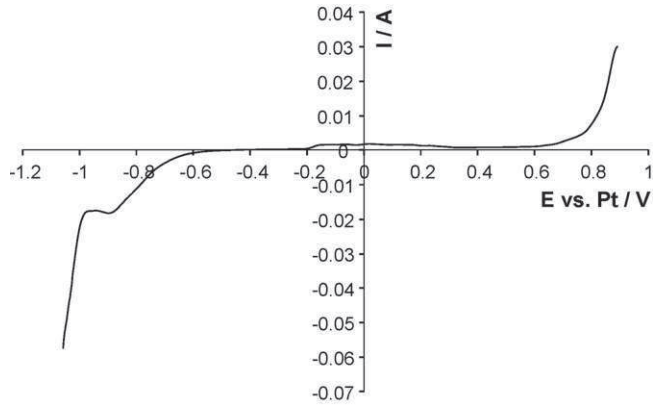

Fig. 14. Linear sweep voltammetry of LiF–CaF_2–Th(IV) (6.77×10^{-2} mol kg^{-1}) on liquid Bi electrode at 5 mV s^{-1} and 840 °C. Auxiliary el.: vitreous carbon; comparison el.: Pt.

A comparison of cyclic voltammograms of the LiF–CaF_2–ThF_4 system on Mo and liquid Bi electrodes, at 100 mV s^{-1}, is presented in Fig. 13. The cathodic limit observed on the curve plotted on Bi, at around −1 V vs. Pt, is attributed to a Bi–Li alloy formation, according to the Bi–Li phase diagram [38]. Prior to the solvent reduction, a small shoulder is observed at −0.9 V vs. Pt. This cathodic peak is enhanced at lower scan rate (5 mV s^{-1}), in conditions close to linear sweep voltammetry, as shown in Fig. 14. This cathodic peak was assumed to be the reduction of Th(IV) into Bi–Th alloys at the surface of the liquid Bi electrode due to its depolarisation. In order to validate this assumption, a potentiostatic electrolysis has been performed at the peak potential (−0.9 V vs. Pt). At the end of the run, the Bi pool was taken out of the cell, cooled and then compacted in a pellet. The radioactive activity measured from the Bi pellet indicated that thorium was present in the Bi phase.

4. Conclusions

From the joint results of the electrochemical study, it has been shown that Th ions dissolved in the LiF–CaF_2 eutectic are reduced into metallic Th on inert electrode, in a single diffusion-controlled step exchanging 4 electrons (Th(IV) + 4e$^-$ = Th). The diffusion coefficients have been determined in the 810–920 °C temperature range.

This study provides relevant information regarding the chemical behaviour of dissolved Th(IV). Indeed, if one of the three reaction (oxide precipitation, electrodeposition on Ni or Bi cathode) is applied for the extraction of lanthanides, Th(IV) will react as follows:

(i) In the case of an oxide addition in the salt, a soluble thorium(IV) oxifluoride compound, $ThOF_2$, forms. An excess of oxides leads to the precipitation of ThO_2, which can be easily separated from the melt thanks to a noticeable difference of density.
(ii) Using a solid nickel electrode, thorium is electrodeposited into the form of Th–Ni alloys. In this case the Th reduction potential is shifted to a potential about 0.7 V less cathodic than on inert electrode.
(iii) On liquid Bi electrode, the depolarisation of the Th(IV) reduction is around 0.7 V.

The next step of this study will be to assess whether the reactions evidenced in the present work can be applied for the purpose of the Th/lanthanides separation. The main point will be to evaluate if the precipitation of lanthanides or their extraction by electrodeposition can be performed without removing Th(IV) from the molten salt.

Acknowledgment

Financial support for this project was provided by the French CNRS PACEN Program (GDR PARIS and PCR ANSF).

References

[1] B. Abrams, S. Levy, D. Chapin et al. A technology roadmap for generation IV nuclear energy systems, issued by the US DOE Nuclear Energy Research Advisory Committee and the Generation IV International Forum, December 2002, available via http://gif.inel.gov/roadmap/pdfs/gen_iv_roadmap.pdf.
[2] E. Merle-Lucotte, D. Heuer, M. Allibert, X. Doligez, V. Ghetta, Proceedings of the GLOBAL 2009 Conference, Paris, France, 6–11 September 2009, 1864.
[3] H.G. MacPherson, Nucl. Sci. Eng. 90 (1985) 374.
[4] P.N. Haubenreich, J.R. Engel, Nucl. Appl. Technol. 8 (1970) 118.
[5] M. Perry, Ann. Nucl. Energy 2 (1975) 809.
[6] J.R. Engel, H.F. Bauman, J.F. Dearing, W.R. Grimes, E.H. McCoy, W.A. Rhoades, ORNL/TM-7207, Oak Ridge National Laboratory, 1980.
[7] R.C. Robertson, ORNL-4541, in: Oak Ridge National Laboratory Report, 1971.
[8] E. Walle, J. Finne, G. Picard, S. Sanchez, O. Conocar, J. Lacquement, Proceedings of the GLOBAL 2003 Conference, New Orleans, USA, November 16–20, 2003.
[9] S. Delpech, E. Merle-Lucotte, D. Heuer, M. Allibert, V. Ghetta, C. Lebrun, X. Doligez, G. Picard, J. Fluor. Chem. 130 (2009) 11.

[10] T. Yanagi, K. Sakoda, K. Tsuji, Technology Reports of the Osaka University 28 (1978) 319.
[11] M.V. Smirnov, Ya.V. Kudyakov, Electrochim. Acta 28 (1983) 1339.
[12] D. Inman, G.J. Hills, L. Young, J.O.M. Bockris, Ann. N. Y. Acad. Sci. 79 (1960) 803.
[13] R. Srinivasan, S. Flengas, Can. J. Chem. 42 (1964) 1315.
[14] L. Martinot, F. Caligara, At. Energy Rev. 11 (1973) 1.
[15] L. Martinot, J. Radioanal, Nucl. Chem. Lett. 103 (1986) 357.
[16] L. Cassayre, J. Serp, P. Soucek, R. Mamlbeck, J. Rebizant, J.P. Glatz, Electrochim. Acta 52 (2007) 7432.
[17] F.R. Clayton, G. Mamantov, D. Manning, J. Electrochem. Soc. 121 (1974) 86.
[18] C.F. Baes, J. Nucl. Mater. 149 (1974) 51.
[19] L. Martinot, Molten-salt chemistry of actinides, in: A.J. Freeman, C.J. Keller (Eds.), Handbook on the Physics and Chemistry of the Actinides, 243, Elsevier Science Publishers, 1991.
[20] P. Chamelot, P. Taxil, B. Lafage, Electrochim. Acta 39 (1994) 2571.
[21] L. Massot, P. Chamelot, F. Bouyer, P. Taxil, Electrochim. Acta 47 (2002) 1949.
[22] Y. Berghoute, A. Salmi, F. Lantelme, J. Electroanal. Chem. 365 (1994) 171.
[23] A.J. Bard, R.L. Faulkner, Electrochemistry: Principles, Methods and Applications, Wiley Ed., New York, 1980.
[24] L. Ramalay, M.S. Kraus, Anal. Chem. 41 (1969) 1362.
[25] L. Ramalay, M.S. Kraus, Anal. Chem. 41 (1969) 1365.
[26] J.G. Osteryoung, J.J. O' Dea, Electroanal. Chem. 14 (1986) 209.
[27] P. Chamelot, P. Palau, L. Massot, A. Savall, P. Taxil, Electrochim. Acta 47 (2002) 3423.
[28] P. Chamelot, B. Lafage, P. Taxil, Electrochim. Acta 43 (1997) 607.
[29] K. Serrano, P. Taxil, J. Appl. Electrochem. 29 (1999) 497.
[30] C. Hamel, P. Chamelot, P. Taxil, Electrochim. Acta 49 (2004) 4467.
[31] C. Bessada, O. Pauvert, A. Rakhmatullin, D. Zanghi, H. Matsuura, Proceedings of the 8th International Symposium on Molten Salts Chemistry and Technology, Kobe, Japan, 2008.
[32] R.K. Jain, H.C. Gaur, B.J. Welch, J. Electroanal. Chem. 79 (1977) 211.
[33] H.B. Herman, A.J. Bard, Anal. Chem. 35 (1963) 1121.
[34] W. Weppner, R.A. Huggins, J. Electrochem. Soc. 124 (1977) 1569.
[35] P. Taxil, J. Less Common Met. 113 (1985) 89.
[36] F. Lantelme, J. Chevalet, J. Electroanal. Chem. 121 (1981) 311.
[37] L. Massot, P. Chamelot, P. Taxil, Electrochim. Acta 50 (2005) 5510.
[38] Binary Alloys Phase Diagram, 2nd ed., ASM International, Materials Park, 1996.
[39] P. Chamelot, L. Massot, C. Hamel, C. Nourry, P. Taxil, J. Nucl. Mater. 360 (2007) 64.
[40] J. Serp, P. Lefebvre, R. Malmbeck, J. Rebizant, P. Vallet, J.P. Glatz, J. Nucl. Mater. 340 (2005) 266.
[41] T. Nishimura, T. Koyama, M. Iizuka, H. Tanaka, Progr. Nucl. Energy 32 (3/4) (1998) 381.